Contact time reduction of droplets bouncing on cylindrical ridges of different size

Matthew Andrew[1], Julia M Yeomans[1*]

[1] *The Rudolf Peierls Centre for Theoretical Physics, 1 Keble Road, Oxford, OX1 3NP, UK*

Abstract

Reducing the contact time of bouncing droplets is relevant to a broad range of industrial applications, such as anti-icing and self-cleaning. Previous work has found that placing cylindrical obstacles on the substrate leads to a reduction in contact time. Here we use experiments and simulations to study in greater detail the effect of varying the obstacle size on the dynamics of the drop bouncing. We find that the contact time is minimised when the radii of the drop and the cylindrical obstacle are comparable.

Introduction

The impact of liquid drops upon surfaces has been studied for many years[1,2] due to both its intrinsic scientific interest and its importance in numerous applications, for example, inkjet printing[3], plant spraying[4], spray cooling[5,6] and water harvesting[7–9]. Improving the efficiency of these processes requires an understanding of the possible results of droplet impact upon surfaces as well as how conditions can be controlled to promote certain behaviours. In particular there have recently been several attempts to devise ways of reducing the time of contact between the drop and the surface by altering the surface geometry[10–17], an improvement of relevance to anti-icing[18–21] and waterproofing[22].

Very recent work has demonstrated novel ways in which droplets bounce on superhydrophobic surfaces with a reduced contact time. In the experiments of Bird *et al.*[10], drops of radius 1.33 mm hit a single ridge of width 150μm on an otherwise flat surface. The impact Weber number $We = \rho v_0^2 R/\sigma = 26$, where ρ is the drop density, R is the drop radius, σ is the surface tension and v_0 is the original velocity of the drop. During spreading the droplet remains approximately circular, but the retraction along the ridge is enhanced because the liquid film is thinner on the ridge. This leads to a pinch-off which splits the drop into two smaller ones. The two separate droplets then retract independently. Note that this contact time reduction was the greatest when the drop hit the ridge centrally and decreased when the drop was off-centre.

In related work, which emphasises the role of the geometry of the drop during retraction, Gauthier *et al.*[12] show that the contact time of a drop hitting small wires placed on the substrate changes with varying impact velocity. For slower impacts, the drop retains a connected shape with lobes linked by bridges, and the contact time is slightly decreased compared to that on a flat superhydrophobic surface. During high-speed impacts, the drop splits into several subdrops in a way depending on the wire geometry. The contact time then scales inversely as the square root of the number of drops produced. Moqaddam *et al.* also found similar results using an entropic lattice Boltzmann simulation method[23].

Recently, Liu *et al.*[11] studied the impact of drops of radius 1.45 mm upon cylinders with radius of curvature between 2 and 10 mm. They found that the drops bounce in an anisotropic shape with a larger extension in the azimuthal direction of the cylinder. This occurs because, as the drop lands, more momentum is transferred into the azimuthal

direction than into the axial direction. The drop then begins retracting along the axial direction whilst remaining extended in the azimuthal direction. The retraction force acting on the rim remains constant and flows around the rim keep the mass of the incoming rim small leading to a faster retraction and subsequent lift-off.

Thus for droplet impacts on surface obstacles much smaller[10,12] or larger[11] than the drop size, the contact time is reduced compared to that on a symmetric surface[24,25]. Here we use simulations and experiments to study droplet bouncing on a semi-cylindrical ridge of varying size on an otherwise flat surface. We show how the contact time varies with ridge radius, hence unifying the understanding of drop bouncing dynamics on anisotropic obstacles. In particular, we show that the maximum contact time reduction is obtained when the drop and obstacle are of similar size.

Methods

We use a phase field model to describe the bouncing droplet. The coupled equations of motion are the Cahn-Hilliard equation[26],

$$\frac{\partial \varphi}{\partial t} + \nabla.(\mathbf{u}\varphi) = M\nabla^2\mu, \tag{1}$$

where the composition φ is an order parameter which distinguishes the liquid and gas phases, M is the mobility of the system and μ is the chemical potential, and the Navier Stokes equation,

$$\rho(\frac{\partial \mathbf{u}}{\partial t} + \mathbf{u}.\nabla\mathbf{u}) = -\nabla p - \varphi\nabla\mu + \eta\nabla^2\mathbf{u}, \tag{2}$$

where $\mathbf{u}$ is the velocity, p is the pressure, ρ is the density and η is the dynamic viscosity.

The chemical potential is determined from the free energy of the system

$$F = \int_V \{F_0(\varphi) + \frac{\kappa}{2}[\nabla\varphi]^2\}\, dV + \int_S \{\phi_0 - \phi_1\varphi_s + \phi_2\varphi_s^2 - \phi_3\varphi_s^3 + ...\}\, dS \tag{3}$$

where V and S denote integrating over the volume and the surface respectively. $F_0 = \beta\varphi^2(1-\varphi)^2$ has two minima at $\varphi = 0$ and $\varphi = 1$ leading to the two stable phases. φ_s is the value of the composition on the solid surface and β, κ and ϕ_{0-3} are constants.

The first integral in Eq. (3) corresponds to the free energy of the bulk and the second to the free energy contribution from any solid surfaces present. A Euler Lagrange minimisation of the bulk terms gives the chemical potential

$$\mu = \frac{\partial F_0}{\partial \varphi} - \kappa\nabla^2\varphi. \tag{4}$$

By integrating over the free interface the surface tension between the two phases, σ, is found to be

$$\sigma = \frac{\sqrt{2\kappa\beta}}{6}. \tag{5}$$

Whilst the interface width is given by $\epsilon = \sqrt{8\kappa/\beta}$. At the solid surface a stable boundary condition on C, which minimises the free energy, is given by $\phi_0 = \phi_1 = 0$, $\phi_2 = 1/2\phi_c$ and $\phi_3 = 1/3\phi_c$. Where $\phi_c = -\sqrt{2\kappa\beta}\cos\theta_{eq}$, with θ_{eq} being the equilibrium contact angle of the surface.

Eqs. (1) and (2) are solved using a lattice Boltzmann algorithm developed by Lee and Liu[27] and Connington and Lee[28]. An important advantage of this numerical approach in the present context, is that it is stable for the large density differences between liquid and gas needed to model bouncing. The parameters used, in simulation units, are listed in Table I. These correspond to dimensionless variables, We between 10 and 39 and $Oh = \eta/\sqrt{\rho\sigma R_0} = 0.013$. The drops here are a bit smaller than those seen in many of the experiments due to stability considerations and as we are below the inertial capillary length scale gravity is neglected.

The substrate is a semi-cylindrical ridge of radius R resting on an otherwise flat surface. Our results are reported in terms of the ratio R/R_0 where R_0 is the radius of the liquid drop. The simulation box is $200 \times 200 \times 200$ nodes in size and, as the geometry has two planes of mirror symmetry, reflection boundary conditions are used in two directions. The simulation is initialised with the drop just above the surface, and with an initial velocity which is varied to provide a range of Weber numbers.

Results

Varying ridge size: Fig. 2 shows the variation of the contact time t, normalized by the inertial capillary time $\tau = \sqrt{\rho R^3/\sigma}$, as a function of the ridge radius R, normalized by the initial drop radius R_0, at $We = 21.6$. The blue horizontal line compares the contact time from a simulation upon a flat surface.

For $R/R_0 > 1$, the contact time slowly decreases as the ridge size is reduced. This is because as the ridge radius decreases, corresponding to an increased curvature, the momentum imbalance between the azimuthal and axial directions becomes larger leading to a decrease in the retraction time of the drop. This trend, which is also seen for other Weber numbers, which is in good agreement with the experiments in[11].

Fig. 3 shows snapshots of drop impact on a single cylinder at $We = 5.3$ for the experiments

Table I. Parameters used in the simulations, and the corresponding dimensionless variables.

Quantity	Value (lattice units)	Quantity	Value (lattice units)
Surface tension σ	0.0083	Initial velocity u_i	0.04 - 0.08
Liquid dynamic viscosity η	0.0084	Drop radius R_0	50
Gas dynamic viscosity η_g	0.00019	Cylinder radius R	10 - 120
Liquid density ρ	1	Mobility M	0.94
Gas density ρ_g	0.0012	Gravitational constant g	0
Interface width ϵ	5	Weber number, We	10 - 39
Contact angle θ_{eq}	180	Ohnesorge number, Oh	0.013

and $We = 10$ for the simulations at $R/R_0 = 2.3$. As a result of the momentum imbalance caused by impact with the cylinder the drop retracts first in the axial direction and this leads to a greater retraction force as well as fluid being pumped around the drop so that the axial retraction is enhanced. Once the axial retraction is complete the drop bounces, still extended around the cylinder, with the central portion of the drop being the last to leave the surface[11].

At $R/R_0 \approx 1$ the contact time reaches a minimum and, as the ridge continues to decrease in radius, the contact time begins to increase with a gradient far greater than the reduction seen for larger ridges. Eventually, as expected for very small ridge sizes, the contact time approaches the value for a flat surface. Note that, it becomes non-physical to resolve the obstacle when its size becomes similar to the interface width. In the simulations this sets a limit on the size of features of $R/R_0 \sim 0.1$.

Fig. 4 shows a collision at $We = 5.3$ for the experiments and $We = 10$ for the simulations, at $R/R_0 = 0.4$ in which the drop contacts both the flat part of the surface and the cylindrical ridge. In this case only a part of the drop is on the cylinder so there is a localised retraction along the central strip of the drop whilst the rest of the drop contracts normally. This leads to a central pinch-off, splitting the drop into two through the impact. From this time onwards the drop retracts as two separate droplets, both from the original outer edges of the drops and from the inner edges near the ridge. When the two edges of each droplet meet they lift off.

Note that the time for the central portion of the drop to retract along the ridge decreases as the ridge size is reduced for $R/R_0 < 1$. However in this regime the retraction does not lead immediately to drop lift-off but rather to a drop splitting and the beginning of a second retraction stage. This can be seen more clearly in Fig. 5, in which the retraction time is separated into two contributions. Here, t_1 is the time for the portion of the drop over the cylinder to retract and t_2 is the time for the drop to lift off the surface after this part of the retraction. For large ridges the lift-off corresponds exactly to the retraction over the central ridge. For smaller ridges, however, there is a significant time after the central ridge retraction before the drop lifts off the surface.

Varying impact velocity: Next, we compare the drop bouncing dynamics with larger impact velocities, and hence a larger *We*. Fig. 6 shows a drop impact at $We = 39$ for the simulation case, $R/R_0 = 2.3$, which can be compared to that with $We = 10$ at the same R/R_0 in Fig. 3. The faster collision leads to a enhanced asymmetry during spreading, as expected, as the initial asymmetry is inertially driven. When the drop lifts-off, it splits into three droplets. As seen from Fig. 6, the origin of the splitting is already apparent by $t/\tau = 0.77$ as most of the fluid is gathered in either the central region or at the edges of the drop. The splitting, unlike that seen for smaller obstacles, has little effect on the contact time. This is because the drop lift-off is still driven by the retraction in the axial direction and the drop the breaks up after the bounce.

Fig. 7 shows a collision at $We = 39$ for the simulation case and $R/R_0 = 0.4$. The bouncing pathway should be compared to Fig. 4 for the same size of cylinder for $We = 10$. The main difference is that the shape of the two droplets on either side of the ridge changes significantly. In particular, as can be seen at $t/\tau = 0.77$ in Fig. 7, a butterfly wing configuration is formed. This agrees with experiments following the fast impact of drops upon ridges[12].

Summary

The ways in which drops bounce upon cylindrical ridges varies substantially as the size of the ridge is changed. In particular there are two distinct regions in which increasing the width of the ridge has opposite effects upon the contact time. The key distinguishing factor between them is the extent to which the drop interacts with the flat surface on which the ridge is placed. For larger ridges the drop never contacts the flat surface. The anisotropic curvature of the surface is responsible for the contact time reduction and, as the curvature

is increased, the contact time is reduced. Conversely, for ridges smaller than the drop, retraction along the ridge does not drive bouncing immediately, but rather creates a pinch-off point which leaves two drops on the surface rather than one. The contact time increases as the ridge size is decreased due to the additional time needed for the individual droplets to leave the surface. Thus the maximum contact time reduction occurs for obstacles with curvature similar to that of the drop.

It would be of interest to investigate the extent to which an array of cylinders or a corrugated surface could be used to reduced mean contact time in the more realistic situation of polydisperse droplets. Moreover the obstacle shape will impact the bouncing, particularly for larger obstacles.

Acknowledgements

J.M.Y. acknowledges support from ERC Advanced Grant MiCE. Y. L is grateful for support from Doctoral Scientific Research Foundation of Science and Technology Commission of Liaoning Province, China (no. 201601047), the Fundamental Research Funds for the Central Universities (DUT16TD20) and the National Natural Science Foundation of China (no. 51605073).

References

[1] Yarin, A. L. Drop impact dynamics: Splashing, spreading, receding, bouncing ... *Annu. Rev. Fluid Mech.* **38**, 159–192 (2006).

[2] Josserand, C. & Thoroddsen, S. T. Drop impact on a solid surface. *Annu. Rev. Fluid Mech.* **48**, 365–391 (2016).

[3] Singh, M., Haverinen, H. M., Dhagat, P. & Jabbour, G. E. *Adv. Mater.* **22**, 673–685 (2010).

[4] Matthews, G. A. Electrostatic spraying of pesticides: a review. *Crop Prot.* **8**, 3–15 (1989).

[5] Kim, J. Spray cooling heat transfer: The state of the art. *Int. J. Heat Fluid Flow* **28**, 753–767 (2007).

[6] Srikar, R., Gambaryan-Roisman, C., T.and Steffes, Stephan, P., Tropea, C. & Yarin, A. L. Nanofiber coating of surfaces for intensification of drop or spray impact cooling. *Int. J. Heat Mass Transf.* **52**, 5814–5826 (2009).

[7] Wisdom, K. M. *et al.* Self-cleaning of superhydrophobic surfaces by self-propelled jumping condensate **110**, 7992–7997 (2013).

[8] Ju, J. *et al.* A multi-structural and multi-functional integrated fog collection system in cactus. *Nat. Commun.* **3**, 1247 (2012).

[9] Hou, Y., Yu, M., Chen, X., Wang, Z. & Yao, S. Recurrent filmwise and dropwise condensation on a beetle mimetic surface. *Acs Nano* **1**, 71–81 (2015).

[10] Bird, J. C., Dhiman, R., Kwon, H.-M. & Varanasi, K. K. Reducing the contact time of a bouncing drop. *Nature* **503**, 385–388 (2013).

[11] Liu, Y., Andrew, M., J., L., Yeomans, J. M. & Wang, Z. Symmetry breaking in drop bouncing on curved surfaces. *Nat. Commun.* **6**, 10034 (2015).

[12] Gauthier, A., Symon, S., Clanet, C. & Quéré, D. Water impacting on superhydrophobic macrotextures. *Nat. Commun.* **6**, 8001 (2015).

[13] Lv, C. J., Hao, P. F., Zhang, X. W. & He, F. Drop impact upon superhydrophobic surfaces with regular and hierarchical roughness. *Appl. Phys. Lett.* **108**, 141602 (2016).

[14] Shen, Y. *et al.* Approaching the theoretical contact time of a bouncing droplet on the rational macrostructured superhydrophobic surfaces. *Appl. Phys. Lett.* **107**, 111604 (2015).

[15] Weisensee, P. B., Tian, J., Miljkovic, N. & King, W. P. Wettability and contact time on a biomimetic superhydrophobic surface. *Sci. Rep.* **6**, 30328 (2016).

[16] Liang, Y. *et al.* Wettability and contact time on a biomimetic superhydrophobic surface. *Materials* **10**, 254 (2017).

[17] Patterson, C. J., Shiri, S. & Bird, J. C. Macrotextured spoked surfaces reduce the residence time of a bouncing leidenfrost drop. *J. Phys. Condens. Matter* **29**, 064007 (2016).

[18] Maitra, T. *et al.* Supercooled water drops impacting superhydrophobic textures. *Langmuir* **30**, 10855–10861 (2014).

[19] Stone, H. A. Ice-phobic surfaces that are wet. *ACS Nano* **6**, 6536–6540 (2012).

[20] Mishchenko, L. *et al.* Design of ice-free nanostructured surfaces based on repulsion of impacting water droplets. *ACS Nano* **4**, 7699–7707 (2010).

[21] Lv, J. Y., Song, Y. L., Jiang, L. & Wang, J. J. Bio-inspired strategies for anti-icing. *ACS Nano* **8**, 3152–3169 (2014).

[22] Callies, M. & Quéré, D. On water repellency. *Soft Matter* **1**, 55–61 (2005).

[23] Moqaddam, A. M., Chikatamarla, S. S. & Karlin, I. Drops bouncing off macro-textured super-

hydrophobic surfaces. *arXiv preprint* (2016).

[24] Richard, D., Clanet, C. & Quéré, D. Contact time of a bouncing drop. *Nature* **417**, 811 (2002).

[25] Rayleigh, L. On the capillary phenomena of jets. *Proc. R. Soc. Lond.* **29**, 71–97 (1879).

[26] Fabrizio, C., Lgnacio, P. & Daan, F. Discrete solution of the electrokinetic equations. *J. Phys. Chem.* **121**, 973–986 (2004).

[27] Lee, T. & Liu, L. Lattice boltzmann simulations of micron-scale drop impact on dry surface. *J. Comput. Phys.* **229**, 8045–8063 (2010).

[28] Connington, K. & Lee, T. Lattice boltzmanm simulations of forced wetting transitions of drops on superhydrophobic surface. *J. Comput. Phys.* **250**, 601–615 (2013).

Figure 1 |. Schematic of the cylindrical ridge.

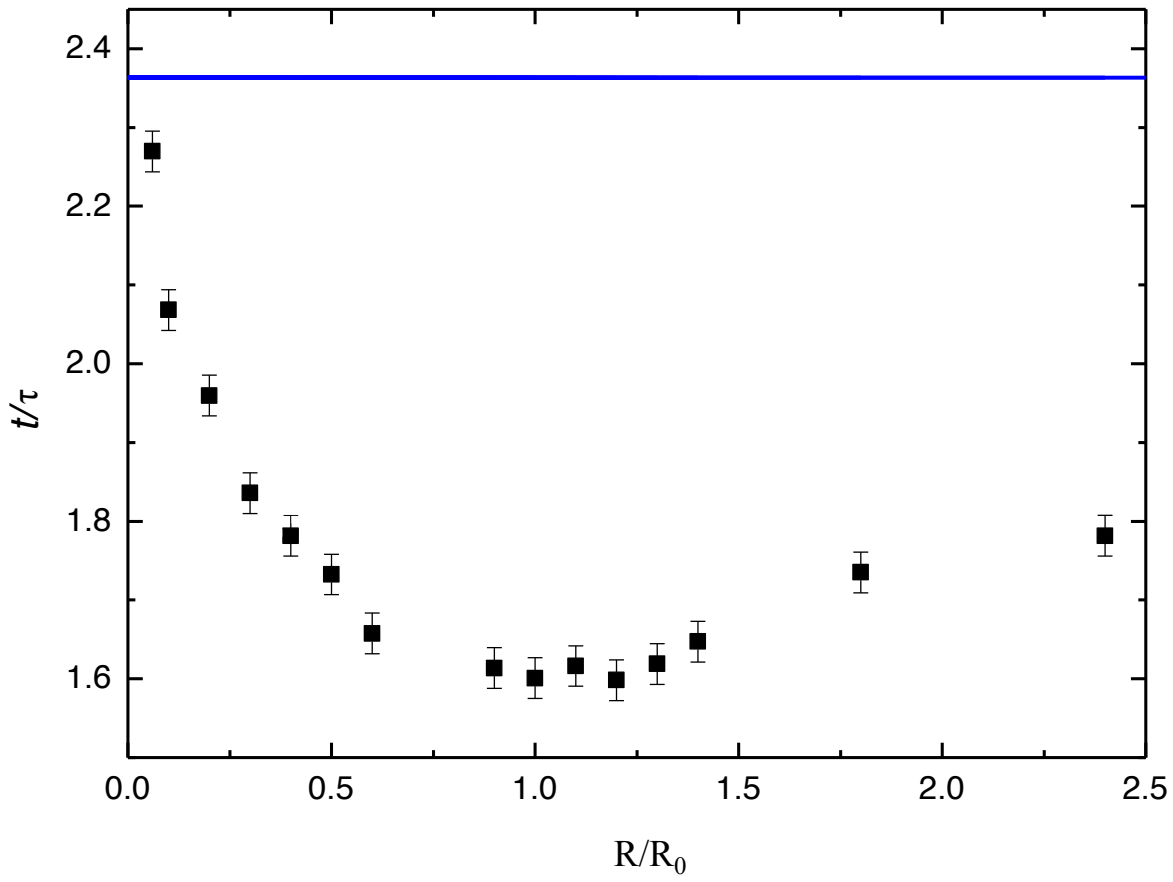

Figure 2 |. Variation of the contact time t, normalised by the inertial capillary time τ, as a function of the cylinder radius R, normalized by the initial drop radius R_0, at $We = 21.6$. The blue horizontal line shows the contact time on a flat surface.

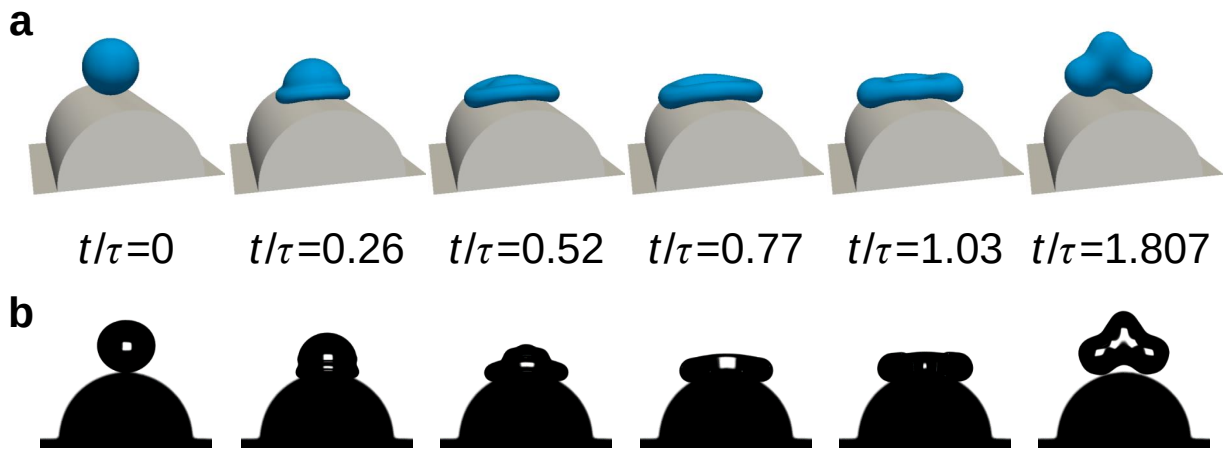

Figure 3 |. Snapshots of a drop impacting on a cylinder at $R/R_0 = 2.3$ comparing (a) simulations at $We = 10$ and (b) experiments at $We = 5.3$.

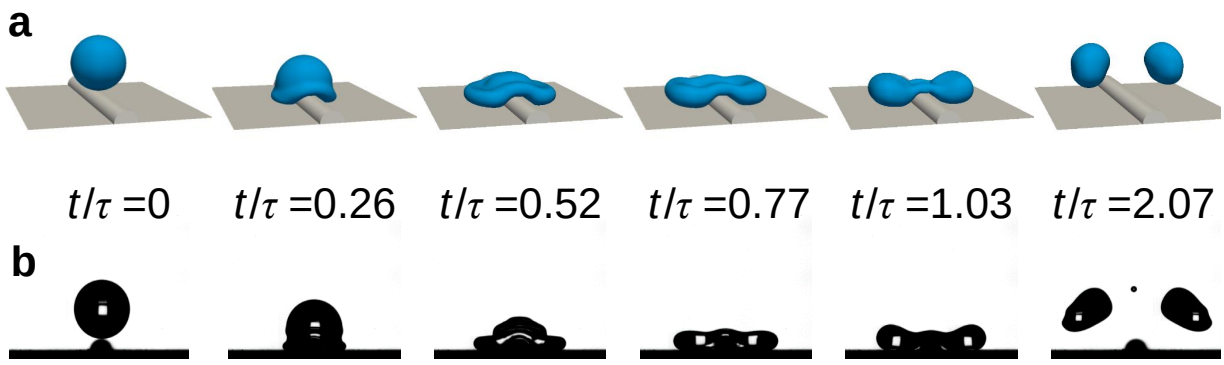

Figure 4 |. Snapshots of a drop impacting on a cylinder at $R/R_0 = 0.4$ comparing (a) simulations at $We = 10$ and (b) experiments at $We = 5.3$. A localised retraction along the ridge causes a central pinch-off, splitting the drop in two midway through the impact. From this time onwards the drop retracts as two separate droplets, both from the original outer edges of the drops and from the inner edges near the ridge. When the two edges of each droplet meet they lift off at $t/\tau = 1.8$.

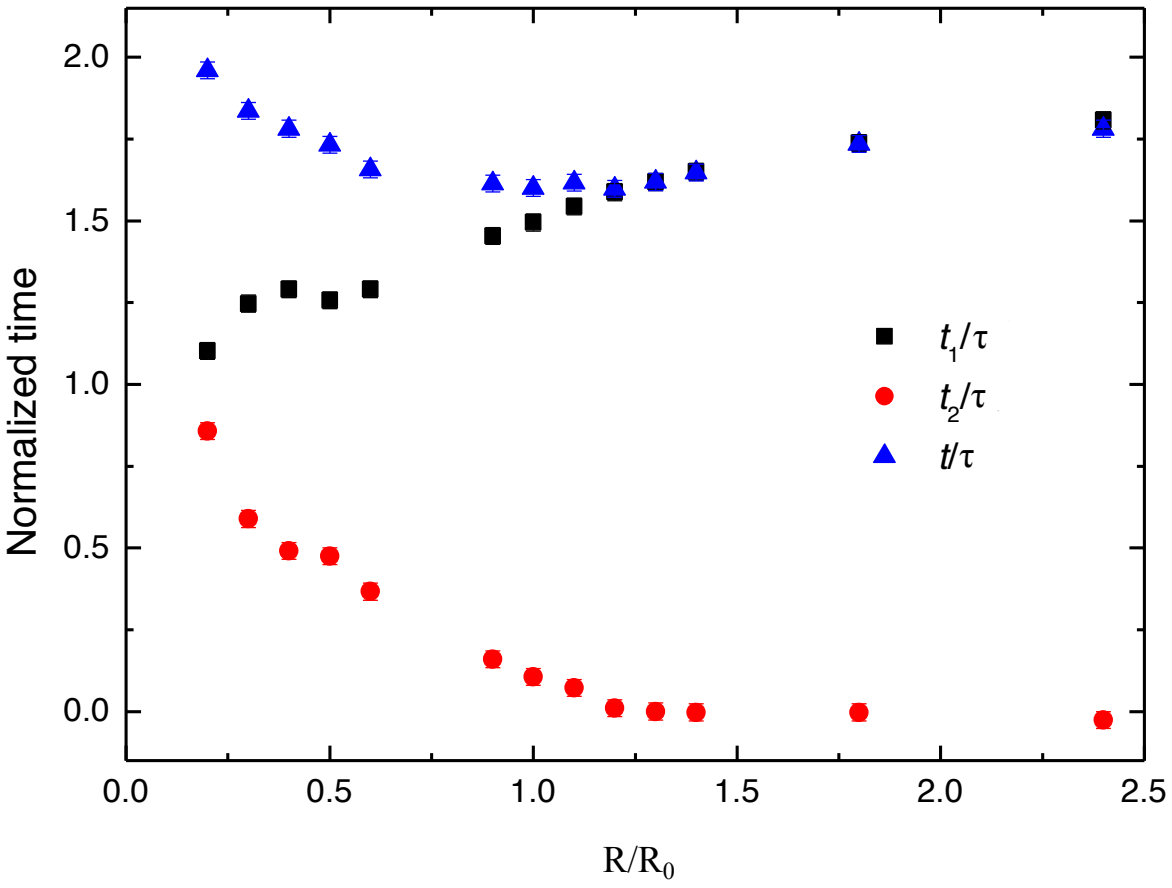

Figure 5 |. Variation of the retraction time over the cylinder, t_1 (black), the time for the drop to lift off after this retraction t_2 (red) and the total contact time $t = t_1 + t_2$ (blue), normalised by the inertial capillary time, as a function of the cylinder radius R, normalized by the initial drop radius R_0, at $We = 21.6$.

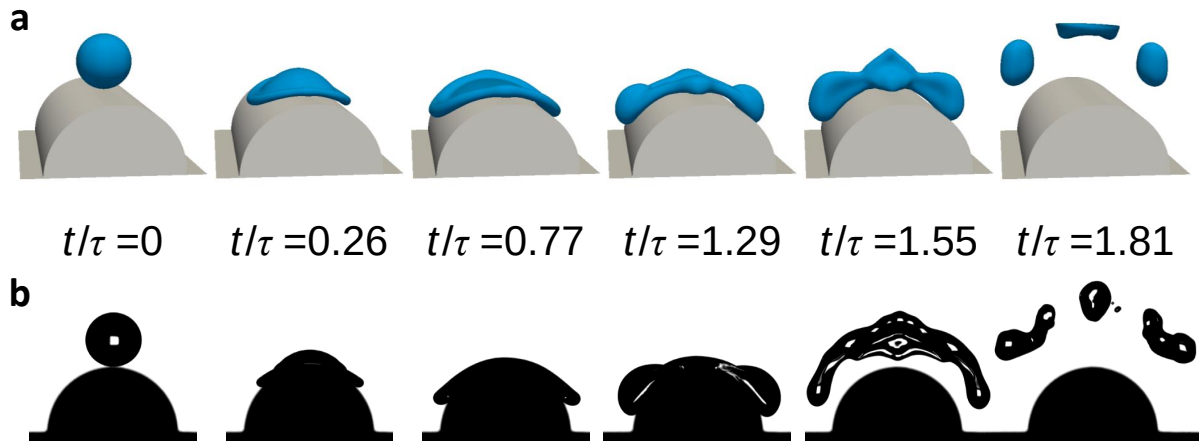

Figure 6 |. Snapshots of a drop impacting on a cylinder at $R/R_0 = 2.3$ comparing (a) simulations at $We = 39$ and (b) experiments at We=23. This faster collision leads to a enhanced asymmetry during spreading, to the extent that the drop almost splits during the spreading step. After the drop lifts-off at $t/\tau = 1.67$, it splits into three droplets.

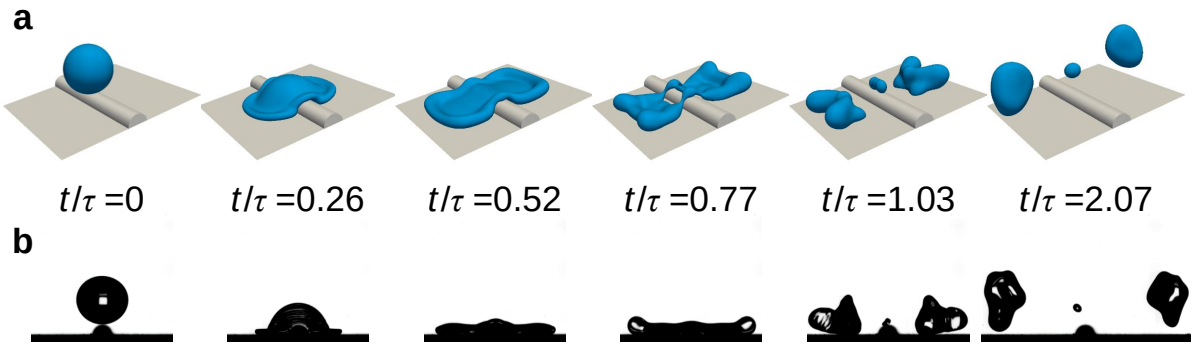

Figure 7 |. Snapshots of a drop impacting on a cylinder at $R/R_0 = 4$ comparing (a) simulations at $We = 39$ and (b) experiments at $We = 23$. At $t/\tau = 0.77$, a butterfly wing configuration is formed.